Freeze-thaw processes correspond to the protection-loss of soil organic carbon through regulating pore structure of aggregates in alpine ecosystems

Ruizhe Wang[1,2], Xia Hu[1,2*]

[1]State Key Laboratory of Earth Surface Process and Resource Ecology, Faculty of Geographical Science, Beijing Normal University, Beijing 100875, China

[2]School of Natural Resources, Faculty of Geographical Science, Beijing Normal University, Beijing 100875, China.

Correspondence to: Xia Hu (huxia@bnu.edu.cn)

Abstract. Seasonal freeze–thaw (FT) processes alter soil formation and causes changes in soil structure in alpine ecosystems. Soil aggregates are basic soil structural units and play a crucial role in soil organic carbon (SOC) protection and microbial habitation. However, the impact of seasonal FT processes on pore structure and its impact on SOC fractions have been overlooked. This study characterized the pore structure and SOC fractions of aggregates during the unstable freezing period (UFP), stable frozen period (SFP), unstable thawing period (UTP) and stable thawed period (STP) in typical alpine ecosystems via the dry sieving procedure, X-ray computed tomography (CT) scanning and elemental analysis. The results showed that pore network of 0.25-2 mm aggregates was more vulnerable to seasonal FT processes than that of > 2 mm aggregates. The freezing process promoted the formation of > 80 μm pores of aggregates. The total organic carbon (TOC), particulate organic carbon (POC) and mineral-associated organic carbon (MAOC) contents of aggregates were high in the stable frozen period and low in unstable thawing period, demonstrating that freezing process enhanced SOC accumulation while early stage of thawing led to SOC loss. The vertical distribution of SOC of aggregates was more uniform in the stable frozen period than in other periods. Pore equivalent diameter was the most important structural characteristic influencing SOC contents of aggregates. In the freezing period, pore structure inhibited SOC loss by promoting the formation of >80 μm pores. In the thawing period, pores of ＜15 μm inhibited SOC loss. Our results revealed that changes in pore structure induced by FT processes could positively contribute to SOC protection of aggregates.

Key words: Seasonal freeze–thaw process, soil aggregate, soil organic carbon, soil pore

1. Introduction

The alpine regions contribute to over 50% of the soil organic carbon (SOC) stock in terrestrial ecosystems, which is 1.5 times higher than the atmospheric carbon pool (Tarnocai et al., 2009). Significant soil carbon emissions from warming-induced permafrost thawing could further provide a positive carbon feedback to climate change (Schuur and Mack, 2018). Freeze–thaw (FT) cycles are main processes of soil formation in alpine regions (Wang et al., 2007). The ongoing global warming has reduced snow cover in winter and decreased the insulations of soils against freezing, which has increased the frequency of FT cycles (Kreyling et al., 2008). Soil aggregates are fundamental soil structural units and favour SOC protection (Oztas and Fayetorbay, 2003; Tan et al., 2014). SOC is preserved by physical protection in the forms of light organic carbon (fLOC), particulate organic carbon (POC) and mineral-associated organic carbon (MAOC). POC is a crucial contributor to soil aggregation and parallels plant-derived carbon into aggregates, and MAOC plays a crucial role in long-term SOC storage (Wang et al., 2020; Witzgall et al., 2021). FT processes may loosen the aggregates' protection of SOC by stimulating substrate release (Song et al., 2017), destroying soil aggregates and stimulating microbial activities (Campbell et al., 2014; Xiao et al., 2019), and the impact is highly dependent on SOC components. For example, FT processes could significantly increase soil soluble carbon content and extractable SOC content but decrease microbial biomass carbon (MBC) content of aggregates (Patel et al., 2021). The increase in microporosity and microbial activity of aggregates induced by FT could decrease the dissolved organic carbon (DOC) concentration (Kim et al., 2023). More frequent FT cycles enhance SOC availability especially in active layers and thus lead to a high risk of greenhouse gas release (Estop-Aragones et al., 2020). However, these related studies were mostly based on simulated laboratory FT experiments. The field FT process is elusive as it contains the complex interactions between soil properties, plant growth and topographic features, which are responsible for differences in the outcomes between laboratory and field conditions (Henry et al., 2007; Deng et al., 2024). Therefore, quantifying the actual dynamics of SOC of aggregates under seasonal FT processes is valuable.

Soil structure refers to the spatial arrangement of solids and voids and controls many important biophysical processes in soils (Rabot et al., 2018). The pore networks of soil aggregates are heterogeneous. FT processes not only affect the stability of soil aggregates but also change

their inner pore characteristics, especially those of the water-filled pores (Wang et al., 2012; Li and Fan, 2014; Starkloff et al., 2017). For example, A decrease in pore connectivity, an increase in elongated porosity and an increase in asymmetrical pores were observed after continuous FT events (Ma et al., 2020; Rooney et al., 2022; Kim et al., 2023). Pore network determines the accessibility of organic matter to microbes and indirectly influence microbial activities, thus determining the magnitude to which the SOC is protected (Ruamps et al., 2013; Kravchenko and Guber, 2018). Interactions between pore structure and SOC fractions of soil aggregates have gained much attention. Pores of 30-75 μm and > 13 μm in size were found to enhance the mineralization of carbon (Lugato et al., 2009; Kravchenko et al., 2015). Pores of > 90 μm and < 15 μm in size were found to support SOC protection (Ananyeva et al., 2013; Quigley and Kravchenko, 2022). 30–150 μm pores are also the preferential places for new carbon inputs and greater abundance of such pores translates into a higher spatial footprint that microbes make on SOC storage capacity (Kravchenko et al., 2019). These distinct correlations demonstrated that the pore-SOC interactions are highly dependent on environmental conditions. In alpine ecosystems, dynamics of SOC can be significantly correlated with the transformation and destruction of aggregates induced by FT processes (Dagesse, 2013). However, the role of pore structure in regulating SOC dynamics in FT processes has not been revealed.

The Qinghai-Tibet Plateau (QTP) has warmed twice the global average rate in recent years with the average temperature being expected to increase by over 2 ℃ before 2070 (Lin et al., 2019). Soils of the QTP are fragile and vulnerable to the global climate change. The depth and duration of FT processes have decreased while the frequency of FT cycles has increased in the QTP (Peng et al., 2017), posing dramatic alterations on the soil pore network (Gao et al., 2020; Yang et al., 2021). Our previous studies have shown that alpine meadow soil aggregates of the QTP had dense pore networks with many elongated pores in them due to frequent FT cycles (Zhao et al., 2020). For typical ecosystems on the QTP, the aggregate protection of SOC was promoted by pores of <15 μm by limiting microbial access and the process was most closely associated with soil moisture content (Wang and Hu, 2023). Aggregate stability has been proved to impact SOC protection on the QTP and thawing-induced SOC loss of aggregates will translate into carbon emissions from the meadow to the atmosphere and exacerbate global warming (Ozlu and Arriga, 2021). Changes in carbon storage depend on relationships between SOC input from litter and root

exudates and output by microbial metabolic activities, and pore structure defines the pathway of substrate movement (Qiao et al., 2023). Overall, the pore structure of aggregates under FT conditions has important implications for predicting carbon turnover projections under global warming (He et al., 2021).

To fill these research gaps, the objectives of the study were: (1) to quantify changes in pore structure and SOC fraction contents of aggregates in typical alpine ecosystems during the seasonal FT process; (2) to investigate the relationships between them and (3) to clarify the role of pore structure on aggregate functions related to SOC protection during seasonal FT processes.

2. Materials and methods

2.1 study sites and sampling

The study was carried out in the Qinghai Lake Watershed (36°15′N-38°20′N, 97°50′-101°20′E), northeastern QTP. The area lies in the cold and high-altitude climate zone, with a mean annual temperature and precipitation of 0.1 ℃ and 400 mm, respectively (Li et al., 2018). Two ecosystems were selected in the study: *Kobresia pygmaea* meadow (KPM) and *Potentilla fruticosa* shrubland (PFS). They are representative terrestrial ecosystems of the Qinghai Lake watershed and account for over 60% of the watershed land area (Hu et al., 2016). One of the main features of these two ecosystems is the mattic epipedon present on the soil surface. Mattic epipedon is the surface layer consisting of a grass felt-like complex formed by the interweaving of live and dead roots of different ages. The layer is soft and significantly enhances nutrient preservation (Hu et al., 2023). The soil type was classified as Gelic Cambisols according to the FAO UNESCO system (IUSS Working Group WRB, 2022). We tried to avoid the simple pseudo replication so that each sampling site has a certain distance with others (> 1 km). Three sites within each ecosystem have similar vegetation conditions. In every FT period, three sampling plots (1 m × 1 m) were set up at each site.

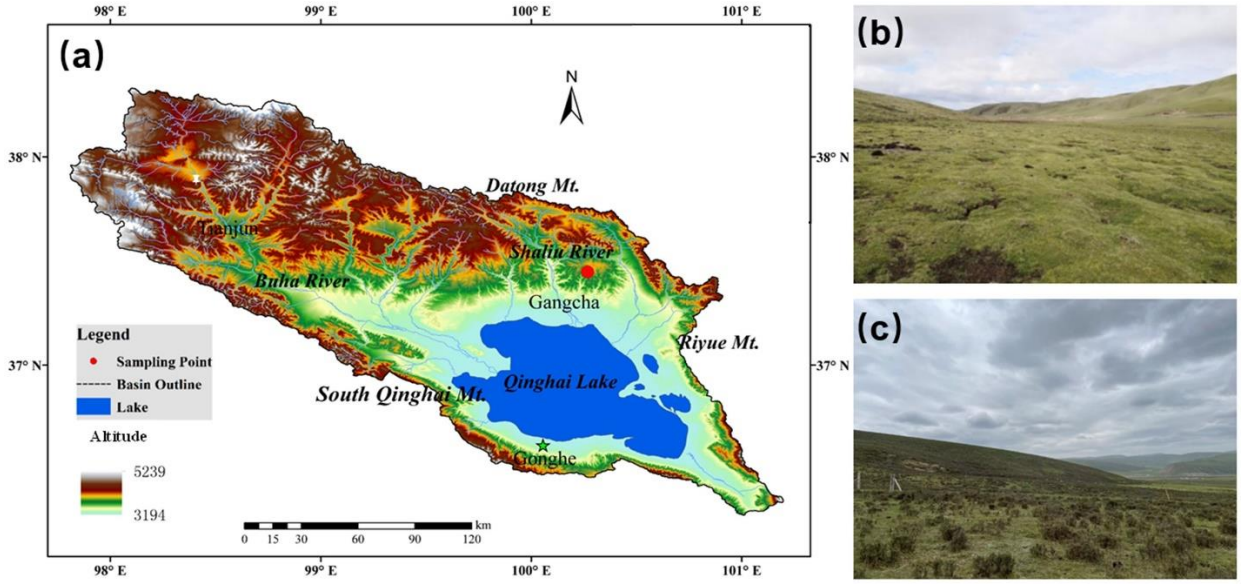

Fig. 1. Location of the sampling site (a) and landscapes of the *Kobresia pygmaea* meadow ecosystem (b) and the *Potentilla fruticosa* shrub ecosystem (c).

The division of seasonal FT periods is based on changes in daily soil temperature (Chen et al., 2021; Wu et al., 2023). The EM-50 soil temperature data for 2019, 2020, and 2021 were obtained at 0.5 Hz with 30 min averages at all three study sites using the ECH2O 5TE sensor (Decagon Devices, USA) (Li et al., 2018). The seasonal freeze–thaw process was divided into four periods in this study: the unstable freezing period (UFP, as soil temperature starts to drop to 0℃), the stable frozen period (SFP, with soil temperature completely blow 0 ℃), the unstable thawing period (UTP, as soil temperature starts to rise above 0 ℃), and the stable thawed period (STP, with soil temperature completely above 0 ℃). The freezing process included the SFP and UFP, while the thawing process included the STP and UTP. Soil samples were taken in October 2021 (representing UFP), January 2022 (representing SFP), May 2022 (representing UFP) and July 2022 (representing SFP).

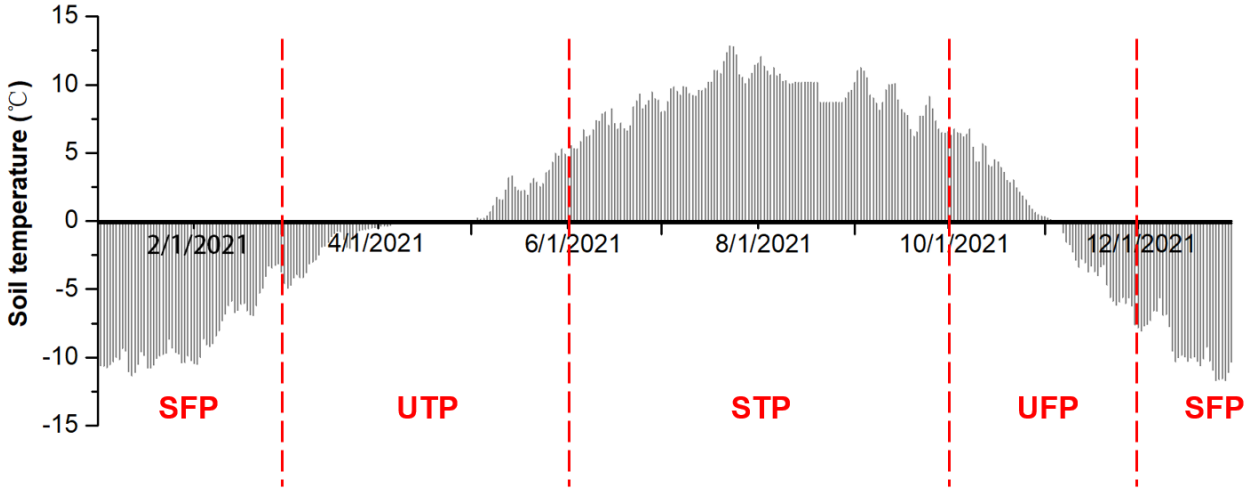

Fig. 2. Daily average soil temperature in 2021 and the classification of freeze–thaw stages (SFP-stable frozen period, UTP-unstable thawing period, STP-stable thawing period and UFP-unstable freezing period).

Soils from three typical profiles in the sampling plots (1 m×1 m) in each site were dug. A total of 18 soil profiles were obtained in every FT period. We classified the soil layers as 0-10 cm, 10-30 cm and 30-50 cm soil layers. Soil cores and bulk soil were collected at each soil layer for aggregate sieving and physiochemical characteristic measurements, respectively. Soil cores were obtained using an 80 mm diameter soil auger and then preserved in an icebox before being sieved in the laboratory. A total of 54 soil cores were collected in every FT period. Nitrile powder-free gloves, a plastic garden trowel, and a small saw were utilized for bulk soil sampling. The basic soil properties of each soil layer at the study site are listed in Table S1. Particle size distribution was determined using the sieve-pipette method (Mako et al., 2019; Zhao et al., 2021). The soil water content as weight was determined using an oven-dried method (Klute, 1986). Soil pH measurements were conducted by an FE20 pH meter (Mettler Toledo, Columbus, USA) from slurries of samples at a soil:water ratio of 1:2.5 (w:w) (Zhao et al., 2020). SOC and TN were determined using a CN 802 elemental analyzer (VELP, Italy). Inorganic carbon was removed from the soil samples using 1 mol/L HCl prior to elemental analysis (Zhang et al., 2017).

2.2 Aggregate sieving

Separation of soil aggregates was performed using the dry sieving method with 0.053, 0.25- and 2-mm sieves from bottom to top. Soil cores were gently broken by hand into 1-cm clods, and then soils were laid out between sheets of brown paper (Schutter and Dick, 2002). Debris such as

gravel and roots were removed from the samples. Two hundred grams of soil was placed on the top sieve and was shaken for five minutes by the sieve shaker (200r/min). Therefore, the aggregates were divided into four categories: large macroaggregates (LMAs, with diameters >2 mm), small macroaggregates (SMAs, with diameters of 0.25~2 mm), microaggregates (mAs, with diameters of 0.053~0.25 mm), and fractions with diameters <0.053 mm. Aggregate fractions of > 2 mm and 0.25-2 mm were weighed and preserved for further analysis.

2.3 CT sanning and image processing

A nanoVoxel-4000 X-ray three-dimensional microscopic CT (Sanying Precision Instruments Co., Ltd., China) was used to scan the soil aggregates with X-ray source parameters of voltage 80 kV and current 50 μA, with which 2800 detailed and low-noise images could be obtained during a 360° rotation. The reconstructed images featured a 3.6 μm spatial resolution and 2800 × 2800 × 1500 voxels. Aggregate fractions of > 2 mm and 0.25-2 mm from all soil layers of the UFP, SFP, UTP and STP periods were scanned (other fractions were too small to separate into a single sample). A total of 144 aggregates were selected and scanned.

Reconstruction of the pore network of aggregates was completed using Avizo 9.0 (Visualization Sciences Group, Burlington, MA). The procedure for image analysis was similar to that described by Wang and Hu (2023). Briefly, the clutters around the aggregates were eliminated using a volume-editing module. Mask extraction was carried out in the segmentation module (Zhao et al. 2020). The soil matrix was selected with the “Magic Wand” tool, and then the “Fill” tool was used to fill the pores for obtaining the aggregate boundary and the mask of the whole aggregate (Zhao and Hu, 2023a). All images were binarily segmented using the histogram thresholding method based on the global thresholding algorithm (Jaques et al., 2021), and pore thresholds were selected for all images.

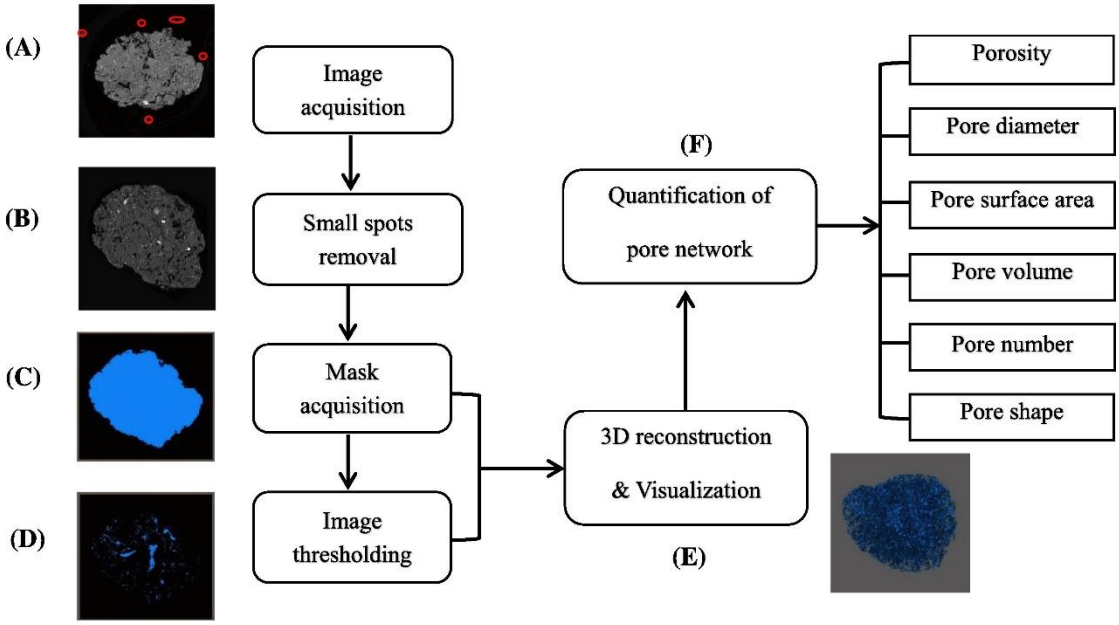

Fig. 3. Procedures used for the visualization and quantification of soil aggregate pore networks. Taken from Zhao et al. (2020) with permission from Elsevier.

The two-dimensional images were transformed into 3D images by Volume Rendering tool in Avizo 9.0 software. The intra-aggregate porosity was calculated using the Volume Fraction tool. After transforming 2D images into 3D images, pore characteristics including the equivalent diameter, volume, number, length, and surface area were calculated using the Label Analysis tool. The pore number density (ND) is defined as the ratio of the pore number (n) to the total volume of the aggregate samples (V):

$$ND = \frac{n}{V} \quad (1)$$

One pore network may consist of several branches of connected pores or just one individual pore. The pore length is the total actual length in all branches. The pore length density (LD) is defined as the ratio of the pore length (L) to the total volume of pores (V) (Yang et al., 2021):

$$\mathrm{LD} = \frac{L}{V} \quad (2)$$

The surface area density (SD) is defined as the ratio of the pore surface area (S) to the total volume of V:

$$SD = \frac{S}{V} \quad (3)$$

To characterize the pore shape, the pore shape factor (SF) was calculated as follows:

$$SF = \frac{A_0}{A} \quad (4)$$

where A_0 represents the surface area of the equivalent sphere of the pores and A is the actual surface area of the pores. SF values closer to 1 indicate a more regular pore shape (i.e., closer to a spherical shape), and smaller values refer to more irregular or elongated pore shapes (Zhou et al., 2012).

The equivalent diameter (EqD) was defined as the diameter of spherical particle with the same volume and was calculated by pore volume:

$$EqD = \sqrt[3]{\frac{6 \times V}{\pi}} \quad (5)$$

Where V represents the volume of pores.

The pores were divided into four classes based on their equivalent diameter: <15, 15–30, 30–80, and >80 μm. According to Lal and Shukla (2004) and Wang and Hu (2023), pores <30, 30–80, and >80 μm are termed micropores, mesopores and macropores, respectively.

2.4 SOC fraction separation

In every FT period, soil aggregate samples were sufficiently ground to pass through a 0.15 mm sieve before their total organic carbon content (TOC) content was measured using the CN 802 elemental analyzer (VELP, Italy).

The determination of SOC fractions, including POC and MAOC, was performed as described by Cambardella and Elliott (1992). Approximately 5 g of each dried aggregate of the LMA and SMA fractions was moved to a 50 mL centrifuge tube and dispersed in 25 mL of a sodium hexametaphosphate (0.5%, w/v) solution by shaking for 18 h in a reciprocating shaker at 120 RMP to ensure that it was evenly blended (Chen et al., 2020; Fu et al., 2023). The dispersed samples were rinsed onto a 53 μm sieve to separate MAOC (particle size <53 μm) and POC (particle size >53 μm) using distilled water until the water stream was clear and free of fine soil particles. After that, samples were transferred to evaporating dishes and dried at 65 ℃ for 48 h to isolate soils which contained POC or MAOC fractions solely (Six et al., 1998). After weighing and sieving, all the fractions' SOC contents were measured using the CN802 elemental analyser (VELP, Italy). The POC and MAOC contents were obtained by multiplying the percentage of each particle size fraction in the soil (Sun et al., 2023).

226 *2.5 Statistical analysis*

227 All statistical analyses except redundancy analysis (RDA) were conducted with IBM's SPSS
228 20 software (SPSS Inc., USA). One-way analysis of variance (ANOVA) followed by Fisher's
229 protected least significance difference (LSD) test was conducted to compare differences between
230 the four seasonal FT periods and between different aggregate fractions. Pearson's correlations
231 were conducted to evaluate the linkages between pore characteristics and SOC fractions of
232 aggregates. Statistical significance was defined at $P < 0.05$. RDA was conducted to determine pore
233 parameters that had a significant impact on SOC fractions and was carried out in R software
234 (http://www.r-project.org) using the vegan package.

235 **3 Results**

236 *3.1 Soil pore characteristics of aggregates*

237 Fig. 4 depicts the pore size distribution of soil aggregates during the seasonal FT process. In
238 the two ecosystems, pores of > 80 μm dominated the pore space in all periods and accounted for
239 over 65% of the total porosity. The contribution of pores of < 15 μm was low in the stable frozen
240 period with 4.39 % in the meadow ecosystem and 5.36 % in the shrubland ecosystem. The volume
241 percentage of pores of > 80 μm was high in the stable frozen period (80.62% in the meadow
242 ecosystem and 87.65% in the shrubland ecosystem) and was significantly higher than that in the
243 UTP (74.17% in the meadow ecosystem and 78.53% in the shrubland ecosystem) and the STP
244 (67.18% in the meadow ecosystem and 80.96% in the shrubland ecosystem). The results showed
245 that freezing process enhanced the formation of pores of > 80 μm while thawing contributed to the
246 increase in porosity of pores of <15 μm.

247

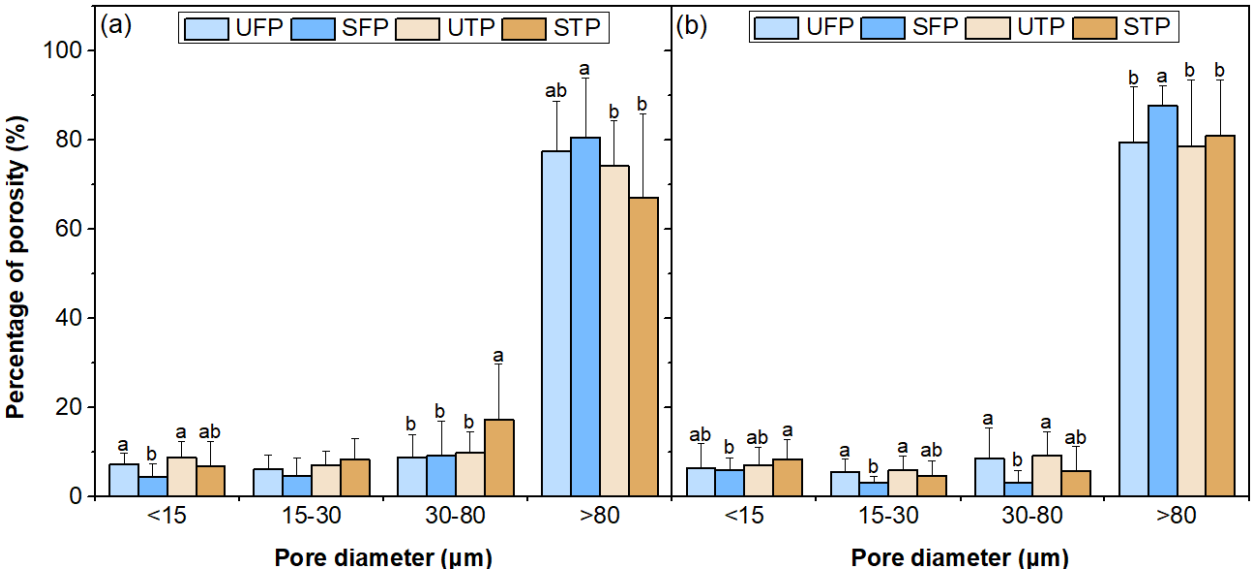

Fig. 4. Pore size distribution (by pore diameter) of soil aggregates in the (a) meadow ecosystem and (b) shrubland ecosystem during the seasonal FT process. Bars represent the mean ± standard error (n=18). Different lowercase letters denote significant differences among pore volume percentages in different FT periods ($P<0.05$).

The characteristics of the pores of aggregates during the seasonal FT process are shown in Fig. 5. The seasonal FT process did not significantly affect the EqD (Fig. 5b). The mean pore volumes of 0.25-2 mm aggregates in the freezing period (3.76×10^3 μm³ and 3.14×10^3 μm³ in the meadow and shrubland ecosystems respectively) were significantly higher than those in the thawing period (2.30×10^3 μm³ and 2.24×10^3 μm³ in the meadow and shrubland ecosystems respectively), while no significant difference was observed for > 2 mm aggregates (Fig. 5c). In the meadow ecosystem, the pore length density of the 0.25-2 mm aggregates was 1.68×10^{-2} μm μm^{-3} in thawing period, which was 1.71 times higher than that in the freezing period (0.98×10^{-2} μm μm^{-3}). In the shrubland ecosystem, pore surface area density and length density of 0.25-2 mm aggregates were 0.0553 μm^2 μm^{-3} and 2.37×10^{-4} μm μm^{-3}, respectively, both significantly higher than those in the freezing period (0.0404 μm^2 μm^{-3} and 1.81×10^{-4} μm μm^{-3} for surface area density and length density, respectively). Overall, seasonal FT processes mainly led to changes in the pore characteristics of 0.25-2 mm aggregates rather than those of > 2 mm aggregates.

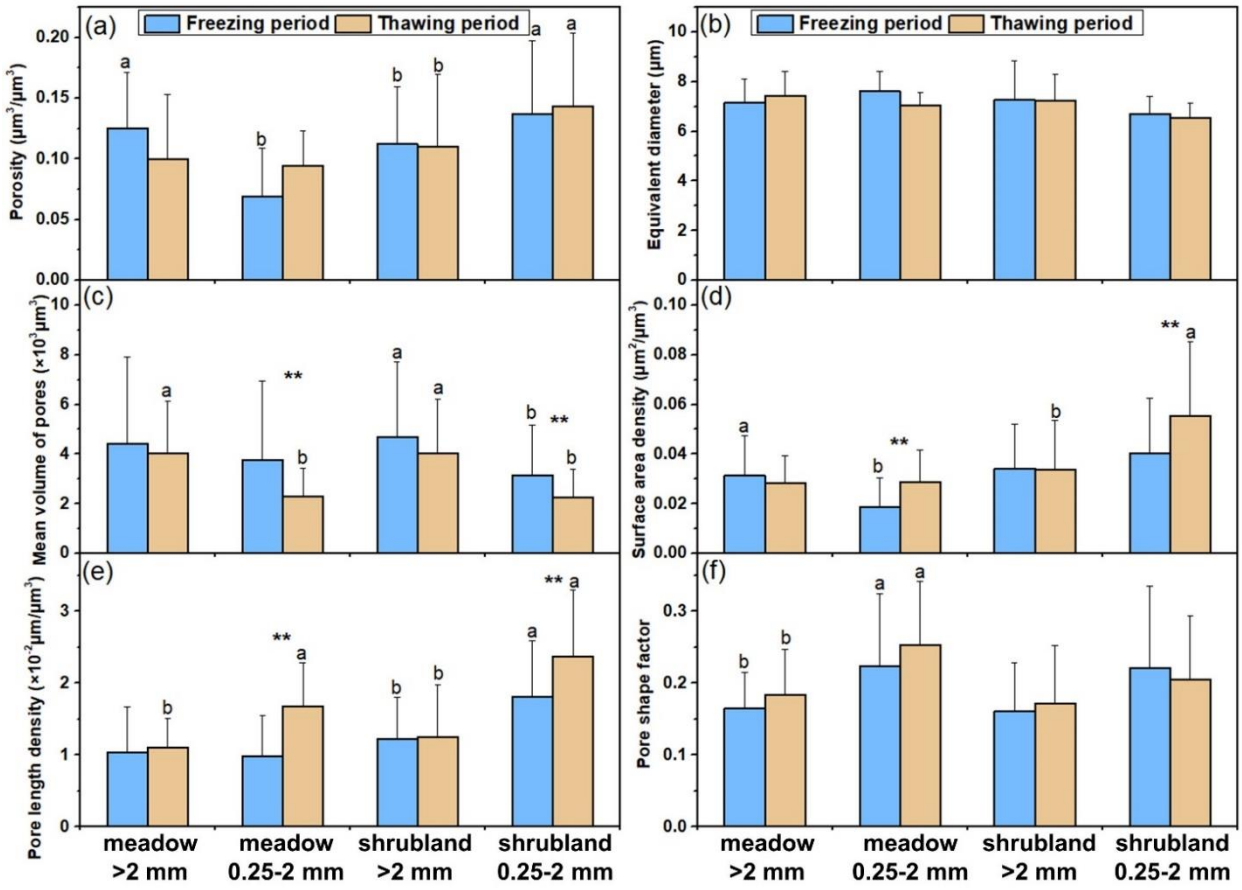

Fig. 5. Pore characteristics of soil aggregates during the seasonal FT process. (a) porosity, (b) pore equivalent diameter, (c) mean volume of pores, (d) pore surface area density, (e) pore length density and (f) pore shape factor. Bars represent the mean ± standard error (n=9). ** represents significant differences between pore characteristics in freezing period and thawing period ($P<0.05$). Different lowercase letters denote significant differences between pore characteristics of >2 mm aggregates and 0.25-2 mm aggregates ($P<0.05$).

3.2 SOC fraction contents of aggregates

The SOC fraction contents (TOC, POC and MAOC) of aggregates during the seasonal FT process is shown in Fig. 6. Generally, in the two ecosystems, the TOC contents of aggregates peaked in the stable frozen period, ranging from 57.33 g/kg to 60.28 g/kg (Fig. 6a). The following unstable thawing period demonstrated the dramatic decline in TOC contents of > 2 mm (dropped by 37.73% and 32.95% in the meadow and shrubland ecosystems, respectively) and 0.25-2 mm aggregates (dropped by 45.57% and 39.43% in the meadow and shrubland ecosystems, respectively).

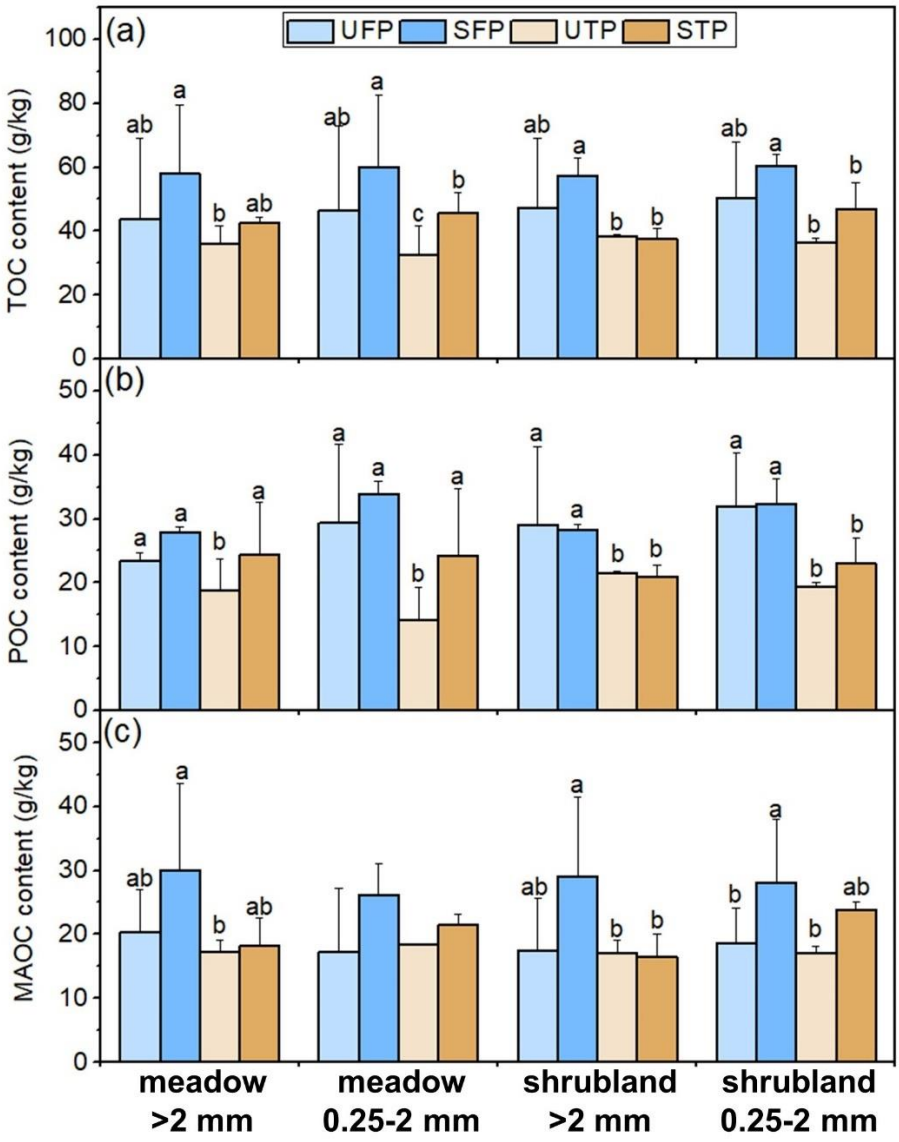

Fig. 6. Changes of SOC content (a-TOC, b-POC and c-MAOC) of soil aggregates during the seasonal freeze–thaw process. Bars represent the mean ± standard error (n=9). Different lowercase letters denote significant differences among SOC contents in different FT periods ($P<0.05$).

Note: UFP-unstable freezing period, SFP-stable frozen period, UTP-unstable thawing period, STP-stable thawed period.

Changes in contents of POC and MAOC were similar to those of TOC (Fig. 6b and 6c). In the meadow ecosystem, the POC contents were high in the stable frozen period (27.90 g/kg for > 2 mm aggregates and 33.77 g/kg for 0.25-2 mm aggregates) and the dramatic decline existed in the unstable thawing period (32.69% for > 2 mm aggregates and 58.01% for 0.25-2 mm aggregates) (Fig. 6b). The MAOC content of > 2 mm aggregates was 29.99 g/kg in the stable frozen period, which was 1.74 times higher than that in the unstable thawing period (17.28 g/kg) (Fig. 6c). In the

shrubland ecosystem, POC contents in freezing periods were significantly higher than those in thawing periods (Fig. 6b). The unstable thawing process led to significant loss in MAOC compared with the stable freezing period (41.54% for > 2 mm aggregates and 39.14% for 0.25-2 mm aggregates) (Fig. 6c). Therefore, freezing increased SOC concentration and the beginning of thawing led to a significant loss of SOC.

The changes in the coefficient of variation (CV) of SOC content during the seasonal FT process, which depicted the variation in the SOC of aggregates from different soil depths, were shown in Table 1. In the two ecosystems, the CV values in the stable frozen period (0.20 for the meadow ecosystem and 0.22 for the shrubland ecosystem) were significantly lower than those in other periods. These results revealed that the freezing process featured a more uniform distribution of SOC across different soil layers.

Table 1 Coefficient of variation (CV) of SOC content of aggregates in all soil layers during the seasonal FT process

Ecosystem	Seasonal FT periods			
	UFP	SFP	UTP	STP
meadow	0.38±0.12a	0.20±0.07b	0.47±0.19a	0.56±0.21a
shrubland	0.46±0.16a	0.22±0.09b	0.34±0.17a	0.34±0.13a

Note: Bars represent the mean ± standard error (n=6). Different lowercase letters denote significant differences in CV of different FT periods.

3.3 Relationships between pore structure and SOC fractions of aggregates

In the freezing period, no correlations were observed between SOC fractions and pore parameters while pore size distribution had significant impact on SOC content. The TOC and MAOC contents were both positively correlated with pores of > 80 μm (P=0.039 and P=0.041, respectively) but negatively correlated with pores of 15-30 μm (P=0.010 and P=0.013, respectively). In the thawing period, the POC content was positively correlated with pores of <15 μm (P=0.049). The TOC and MAOC contents were both positively correlated with pore length density (P=0.045 and P=0.006, respectively).

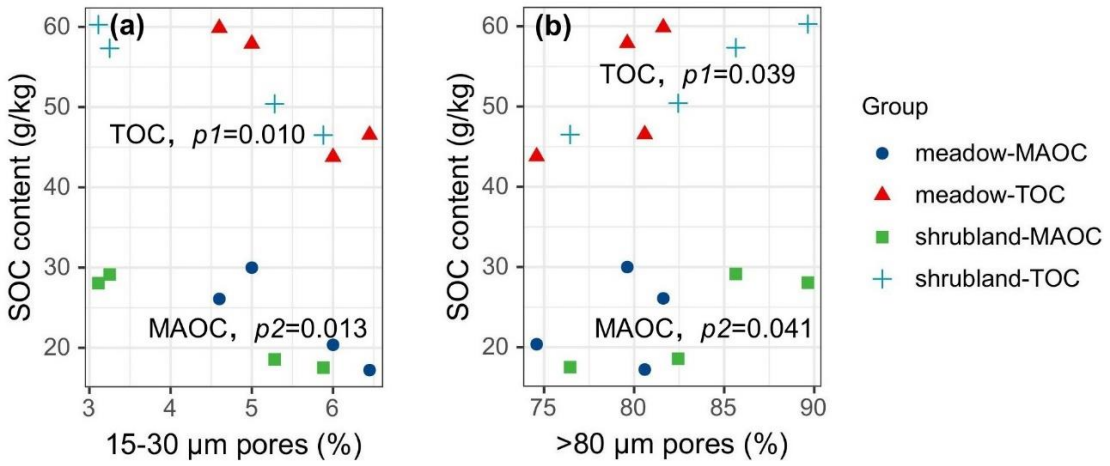

Fig. 7. Scatter plots of relationships between (a) SOC content and 15-30 μm pores and (b) SOC content and > 80 μm pores in the freezing process.

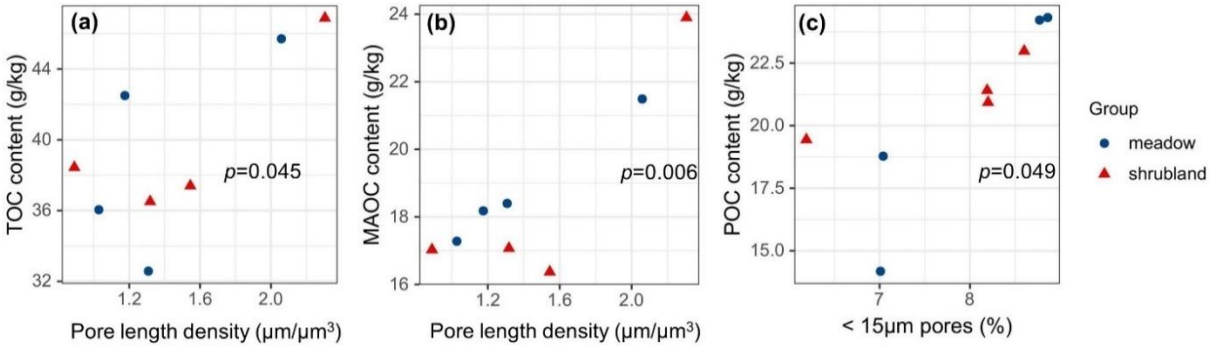

Fig. 8. Scatter plots of relationships between (a) TOC content and pore length density, (b) MAOC content and pore length density and (c) POC content and < 15 μm pores in the thawing process.

RDA was used to explain the relationship between the pore parameters and SOC fractions during the seasonal FT process (Supplementary Fig. 1). In the freezing period, a total of 53.29% of the SOC variation could be explained by pore characteristics. Pore EqD had a significant impact on SOC content (P=0.01). In thawing period, 52.90% of the SOC variation, with 50.99% on Axis 1 and 1.91% on Axis 2, was explained by pore characteristics. Pore surface area and EqD played important roles in SOC dynamics of aggregates (P=0.01 and P=0.04, respectively).

4 Discussion

Our results demonstrated that the volume percentage of > 80 μm pores of aggregates was high in the stable frozen period. This finding is consistent with related results, which showed that

FTresulted in an increase in macroporosity (Wu and Hu, 2024). Ma et al. (2020) found volume percentage of pores of > 100 μm in aggregates increased from 62.39% to 96.53% after 20 times FT cycles. During the freezing process, pore-scale heterogeneities cause pressure gradients and the seepage of water from smaller to larger pores (Rempel and vam Alst, 2013), and this process enhances the expansion of force heave (Skvortsova et al., 2018). Freezing could also increase pore size by forming new connections among adjacent pores (Ma et al., 2020). The increase in pore size and porosity could loosen the aggregate stability and increase pore air content, thus increasing the air pressure and enhancing expansion (Lugato et al., 2010; de Jesus Arrieta Baldovino et al., 2021). We also found that the seasonal FT process mainly affects the pore characteristics of 0.25-2 mm aggregates rather than those of > 2 mm aggregates, especially in the pore surface area density and length density. Zhao and Hu (2023a) reported a similar significant change in pore surface area density of 0.25-1 mm aggregates after FT cycles. Changes in surface area density and pore length density or pores might be associated with pore shape. In the freezing period, the frost heave force of water is anisotropic, which increases the pore length and decreases the surface area(Rooney et al., 2022). In summary, freezing increased the pore volume and the impact of seasonal FT processes on pore characteristics is dependent on aggregate size.

In our study, contents of SOC fractions were all high in the stable frozen period and low in the unstable thawing period. Huang et al. (2021) found that the TOC content of aggregates was high in January and February and showed a significant decrease in March due to FT processes. Many studies have also reported the SOC loss at the beginning of the thawing period at regional scales (Song et al., 2014; Song et al., 2020). This phenomenon can be explained by litter accumulation and suppressed microbial activities in freezing periods (Han et al., 2018), as well as the aerobic environment intensifying SOC mineralization during thawing (Liu et al., 2018; Liu et al., 2021). So, the freezing process promoted SOC accumulation while the thawing process induced a loss of SOC. Freezing also resulted in a more uniform distribution of SOC across different soil layers. This finding corresponds to Zhao and Hu (2023), which proposed the buffered difference in microbial biomass between soil horizons in the frozen period. The phenomenon may be attributed to differences in external disturbances and SOC turnover rates from topsoil to deep soil (Wang et al., 2022). These indicated the positive effect of freezing on vertical nutrient distribution, which lacks investigations so far.

Among all pore characteristics, equivalent diameter explained most in the SOC variations (Supplementary Fig. 1). In the freezing period, pores of 15-30 μm had negative impact on SOC protection, this was consistent with our previous results (Wang and Hu, 2023). Pores of 15–30 μm are probably suitable habitat for soil microbes and support their activity, where greater SOC decomposition takes place (Kravchenko & Guber, 2017; Liang et al., 2019). Pores of >80 μm favoured SOC protection of aggregates. As the period was featured by SOC accumulation (especially residue entry), Pores of > 80 μm serve as primary sites for residue entry and are promoted by microbial materials and SOC, which enhance soil aggregation and thus drive much SOC to be protected (Ananyeva et al., 2013; Dal Ferro et al., 2014; Zhang et al., 2023). Freezing promoted the formation of these pores which were conducive to organic matter entry into aggregates. In the thawing period, pores of <15 μm inhibited the POC loss. Previous studies proved that these pores reduced SOC decomposition via limiting microbial access and shifting microbial metabolism to less efficient anaerobic respiration (Strong et al., 2004; Keiluweit et al., 2017). On the QTP, the positive impact of soil moisture on SOC protection has been revealed in both aggregate scale and landscape scale (Ma et al., 2022; Wang and Hu, 2023). The thawing process is accompanied by an increase in microbial activity and moisture availability, pores of <15 μm are able to hold water surrounding the soil particles (Kim et al., 2021). Therefore, POC associated with these pores was less vulnerable to microbial processing and desorption due to equilibration with the more frequently exchanged soil solution (Schluter et al., 2022). The protection promotes the consequent transport of POC towards mineral sorption and thus contributes to the long-term SOC storage (Vedere et al., 2020). Overall, the FT-induced pore structure posed a positive impact on SOC protection in that: pores of > 80 μm promoted by freezing serve as primary sites for organic matter entry, while pores of <15 μm promoted by thawing inhibited POC decomposition through holding moisture.

In this study, we explored changes in the pore structure and SOC fractions of alpine soil aggregates during the seasonal FT process. However, we could not isolate the impact of FT processes on soil structure and functions as impacts from vegetation and climate could not be avoided under field conditions. Therefore, it is necessary to compare the results based on laboratory FT simulations and field sampling in future studies to clarify the importance of FT processes in shaping pore structure and affecting soil functions. Recent studies have clarified the

importance of minerals (e.g., Fe, Al, and their oxides) in microscale SOC protection (Kang et al., 2024; Wang et al., 2024; Zhu et al., 2024). This mechanism can be closely associated with soil moisture and enzyme activities (Li et al., 2023; Hu et al, 2024), while the role of pore structure has not been clarified. Future research needs to further quantify the impact of soil structure on organic carbon, which will enable us to apply the mechanisms we have discovered to landscape scales to improve existing global carbon cycle predictions.

5 Conclusion

The findings of the study revealed that seasonal FT processes regulate pore structure, and SOC concentration of aggregates. The seasonal FT process significantly affected the pore surface area density and length density of 0.25-2 mm aggregates. The freezing period promoted the formation of pores > 80 μm while thawing led to shrinkage of pore space. Freezing enhanced the accumulation of SOC of aggregates and the more uniform distribution of SOC among different soil layers. Thawing witnessed the loss of SOC. The seasonal FT process altered the SOC protection of aggregates via regulating pore size distribution. Pores of > 80 μm promoted by freezing serve as primary sites for organic matter entry, while pores of <15 μm promoted by thawing inhibited POC decomposition through holding moisture. Overall, our study explains the changes in SOC during the freeze-thaw process by innovatively establishing a pathway of FT-pore structure-SOC. In future studies, by incorporating a more variety of factors, we hope the contribution of soil structure to SOC conservation can be upscaled to achieve a more precise global carbon cycle estimation.

Abbreviations

FT: freeze-thaw, UFP: unstable freezing period, SFP: stable frozen period, UTP: unstable thawing period, STP: stable thawed period, EqD: equivalent diameter of pores, SF: shape factor, LMA: large macroaggregate, SMA: small macroaggregate, SOC: soil organic carbon, TOC: total organic carbon, POC: particulate organic carbon, MAOC: mineral-associated organic carbon.

Declarations

Acknowledgements

This study was financially supported by the National Science Foundation of China (Grant number: 42371107) and the Project Supported by State Key Laboratory of Earth Surface Processes and Resource Ecology (2022-TS-03).

CRediT authorship contribution statement

Ruizhe-Wang: Conceptualization; data curation; formal analysis; methodology; writing-original draft; writing-review & editing. Xia Hu: Funding acquisition; investigation; project administration; supervision; writing-review & editing.

Data availability statement

All data generated or analysed during this study are included in this published article [and its supplementary information files.

Conflict of interest statement

The authors declare that they have no known competing financial interests or personal relationships that could have appeared to influence the work reported in this paper.

References

Ananyeva, K., Wang, W., Smucker, A.J.M., Rivers, M.L., Kravchenko, A.N., 2013. Can intra-aggregate pore structures affect the aggregate's effectiveness in protecting carbon? Soil Biology & Biochemistry. 57, 868–875. doi: 10.1016/j.soilbio.2012.10.019

Angasssa, A. Effects of grazing intensity and bush encroachment on herbaceous on species and rangeland condition in southern Ethiopia. Land Degradation Development, 25: 438.451. doi: 10.1002/ldr.2160.

Bronick, C.J., Lal, R., 2004. Soil Structure and management: a review. Geoderma 124, 3–22. https://doi.org/10.1016/j.geoderma.2004.03.005.

Cambardella, C.A., Elliott, E.T., 1992. Particulate soil organic-matter changes across a grassland cultivation sequence. Soil Science Society of American Journal 56(3): 777-783. doi: 10.2136/sssaj1992.03615995005600030017x.

Campbell. J.L., Socci, A.M., Templer, P.H., 2014. Increased nitrogen leaching following soil freezing is due to decreased root uptake in a northern hardwood forest. Global Change Biology 20, 2663–2673. doi: 10.1111.gcb.12532.

Chen, H., Huang, Y., He, K., Qi, Y., Li, E., Jiang, Z., Sheng, Z., Li, X., 2019.Temporal intraspecific trait variability drives responses of functional diversity to interannual aridity variation in grasslands. Ecology and Evolution, 9 (10), 5731-5742. doi: 10.1002/ece3.5156.

Chen, H., Liu, X., Xue, D., Zhu, D., Zhan, W., Li, W., Wu, N., Yang, G., 2021. Methane emissions during different freezing-thawing periods from a fen on the Qinghai-Tibet Plateau: Four years of measurements. Agricultural and Forest Meterology 297, 108279. doi: 10.1016/j.agrformet.2020.108279.

Chen, J., Xiao, W., Zheng, C., Zhu, B. 2020. Nitrogen addition has contrasting effects on particulate and mineral-associated soil organic carbon in a subtropical forest. Soil Biology and Biochemistry 142, 107708. doi: 10.1016/j.soilbio.2020.107708.

Chen, L., Fang, K., Wei, B., 2021. Soil carbon persistence governed by plant input and mineral protection at the regional and global scales. Ecology Letters, 24: 1018-1028. doi: 10.1111/ele.13883.

Chen, Y., Han, M., Yuan, X., Zhou, H., Zhao, x., Schimel, J.P., Zhu, B., 2023. Long-term warming reduces surface soil organic carbon by reducing mineral-associated carbon rather than “free” particulate carbon. Soil Biology and Biochemistry 177, 108905. doi: 10.1016/j.soilbio.2022.108905.

Dagesse, D.F., 2002. Freezing cycle effects on water stability of soil aggregates. Canadian Journal of Soil Science 93(4): 473-483. doi: 10.4141/CJSS2012-046.

Dal Ferro, N., Sartori, L., Simonetti, G., Berti, A., Morari, F., 2014. Soil macro-and microstructure as affected by different tillage systems and their effects on maize root growth. Soil and Tillage Research, 140, 55–65. doi: 10.1016/j.still.2014.02.003.

de Jesus Arrieta Baldovino, J., dos Santos Izzo, R.L., Rose, J.L., 2021. Effects of freeze-thaw cycles and porosity/cement index on durability, strength and capillary rise of a stabilized silty soil under optimal compaction conditions. Geotechnical and Geological Engineering 39, 481-498. doi: 10.1007/s10706-020-01507-y.

Ding J., Chen, L., Zhang, B., 2016. Linking temperature sensitivity of soil CO_2 release to substrate, environmental, and microbial properties across alpine ecosystems. Global Biogeochemistry Cycles, 30 (9), 1310-1323. doi:10.1002/2015gb005333.

Estop-Aragonés, C., Olefeldt, D., Abbott, B. W., Chanton, J. P., Czimczik, C. I., Dean, J. F., Egan, J. E., Gandois, L., Garnett, M. H., Hartley, I. P., Hoyt, A., Lupascu, M., Natali, S. M., O'Donnell, J. A., Raymond, P. A., Tanentzap, A. J., Tank, S. E., Schuur, E. A. G., Turetsky, M., and Anthony, K. W.: As-sessing the Potential for Mobilization of Old Soil Carbon After Permafrost Thaw: A Synthesis of ^{14}C Measurements from the Northern Permafrost Region, Global Biogeochem. Cy., 34, 1–26. doi: 10.1029/2020GB006672, 2020.

Fu, C., Li, Y., Zeng, L., Tu, C., Wang, X., Ma, H., Xiao, L., Christie, P., Luo, Y., 2023. Climate and mineral accretion as drivers of mineral-associated and particulate organic matter accumulation in tidal wetland soils. Global Change Biology 30, e17070. doi: 10.1111/gcb.17070.

Gao, Z., Hu, X., Li, X., Li, Z., 2021. Effects of freeze–thaw cycles on soil macropores and its implications on formation of hummocks in alpine meadows in the Qinghai Lake watershed, northeastern Qinghai-Tibet Plateau. Journal of Soils and Sediments, 21:245-256. doi:10.1007/s11368-020-02765-2.

Han, C., Gu, Y., Kong, M., Hu, L., Jia, Y., Li, F., Sun, G., Siddique, K.H.M., 2018. Responses of soil microorganisms, carbon and nitrogen to freeze-thaw cycles in diverse land-use types. Applied Soil Ecology, 124: 211-217. doi: 10.1016/j.apsoil.2017.11.012.

He, L., Lai, C., Mayes, M.A., Murayama, S., Xu, X., 2021. Microbial seasonality promotes soil respiratory carbon emission in natural ecosystems: a modeling study. Global Change Biology, 27, 3035–3051. doi:10.1111/gcb.15627.

Hu, W., Li, Q., Wang, W., Lin, X., He, Z., Li, G., 2024. Straw mulching decreased the contribution of Fe-bound organic carbon to soil organic carbon in a banana orchard. Applied Soil Ecology 194, 105177. doi: 10.1016/j.apsoil.2023.105177.

Hu, X., Li, Z., Li, X., Liu, L., 2016. Quantification of soil macropores under alpine vegetation using computed tomography in the Qinghai Lake Watershed, NE Qinghai-Tibet Plateau. Geoderma 264, 244–251. doi: 10.1016/j.geoderma.2015.11.001.

Huang, D., Zhou, L., Fan, H., Jia, Y., Liu, M., 2021. Responses of aggregates and associated soil available phosphorus, and soil organic matter in different slope aspects, to seasonal freeze–thaw cycles in Northeast China. Geoderma, 402, 115184. doi: 10.1016/j.geoderma.2021.115184.

IUSS Working Group WRB, 2022. World Reference Base for Soil Resources. International soil classification system for naming soils and creating legends for soil maps, 4th ed. International Union of Soil Sciences (IUSS), Vienna, Austria.

Jaques, V.A.J., Du Plessis, A., Zemek, M., Salplachta, J., Stubianova, Z., Zikmund, T., Kaiser, J., 2021. Review of porosity uncertainty estimation methods in computed tomography dataset. Measurement Science and Technology 32, 12, 122001. doi: 10.1088/1361-6501/ac1b40.

Kallenbach, C.M., Frey, S.D., Grandy, A.S., 2016. Direct evidence for microbial-derived soil organic matter formation and its ecophysiological controls. Nature Communications 7 (1), 1–10. doi: 10.1038/ncomms13630.

Kang, J., Qu, C., Chen, W., Cai, P., Chen, C., Huang, Q., 2024. Organo-organic interactions dominantly drive soil organic carbon accrual. Global Change Biology 30 (1): e17147. doi: 10.1111/gcb.17147.

Keiluweit, m., Wanzek, T., Kleber, M., Nico, P., Fendorf, S., 2017. Anaerobic microsites have an unaccounted role in soil carbon stabilization. Nature Communications 8, 1771. doi: 10.1038/s41467-017-01406-6.

Kim, Y., Hyun, J., Yoo, S., Yoo, J. 2021, The role of biochar in alleviating soil drought stress in urban roadside greenery, Geoderma, 404, 115223. doi: 10.1016/j.geoderma.2021.115223, 2021

Kim, Y., Kim, J., Jung, J., 2023.Responses of dissolved organic carbon to freeze–thaw cycles associated with the changes in microbial activity and soil structure. The Cryosphere 17, 3101–14. doi: 10.5194/tc-17-3101-2023.

Klute, A., 1986. Methods of Soil Analysis: Part 1–Physical and Mineralogical Methods. American Society of Agronomy, Madison.

Kravchenko, A.N., Guber, A.K., 2017. Soil pores and their contributions to soil carbon processes. Geoderma. 287, 31–39. doi: 10.1016/j.geoderma.2016.06.027.

Kravchenko, A.N., Guber, A.K., Razavi, B.S., Koestel, J.K., Quigley, M.Y., Robertson, G.P., Kuzyakov, Y., 2019. Microbial spatial footprint as a driver of soil carbon stabilization. Nature Communications, 10: 3121. doi: 10.1038/s41467-019-11057-4.

Kravchenko, A.N., Negassa, W.C., Guber, A.K., Rivers, M.L., 2015. Protection of soil carbon within macro-aggregates depends on intra-aggregate pore characteristics. Scientific Reports, 5 (1), 1–10. doi: 10.1038/srep16261

Kreyling, J., Beierkuhnlein, C., Pirtsch, K., Schloter, M., Jentsch, A., 2007. Recurrent soil freeze–thaw cycles enhance grassland productivity. New Phytologist Foundation 177:938–945. doi: 10.1111/j.1469-8137.2007. 02309.x

Lal, R., Shukla, M.K., 2004. Principles of Soil physics. Marcel Dekker, New York.

Lavallee, J.M., Soong, J.L., Cotrufo, M.F., 2020. Conceptualizing soil organic matter into particulate and mineral-associated forms to address global change in the 21st century. Global Change Biology, 26(1). doi: 10.1111/gc.14859.

Lemanski, K., Armbruster, M., Bonkowski, M., 2019. Linking soil microbial nutrient limitation to fertilizer regime and sugar beet yield. Plant and Soil, 441, 253–259. doi: 10.1007/s11104-019-04114-w.

Li, G., Fan, H., 2014. Effect of freeze–thaw on water stability of aggregates in a black soil of Northeast China. Pedosphere, 24 (2), 285–290. doi: 10.1016/ S1002-0160(14)60015-1.

Li, R., Luo, H., Yu, J., Luo, Y., He, Y., Deng, S., Deng, O., Shi, D., He, J., Xiao, H., Wang, L., Lan, T., 2023. The importance of moisture in regulating soil organic carbon content based on a comparison of “enzymic latch” and “iron gate” in Zoige Plateau peatland. Catena 225, 107019. doi: 10.1016/j.catena.2023.107019.

Li, X., Yang, X., Ma, Y., Hu, G., Hu, X., Wu, X., Wang, P., Huang, Y., Cui, B., Wei, J., 2018. Qinghai Lake Basin critical zone observatory on the Qinghai-Tibet Plateau. Vadose Zone Journal, 17 (1): 180069. doi: 10.2136/vzj2018.04.0069.

Liao, J., Yang, X., Dou, Y., 2023. Divergent contribution of particulate and mineral-associated organic matter to soil carbon in grassland. Journal of Environmental Management 344, 118536. doi: 10.1016/j.jenvman.2023.118356.

Lin, Z, Gao, Z., Niu, F., Luo, J., Yin, G., Liu, M., Fan, X., 2019. High spatial density ground thermal measurements in a warming permafrost region, Beiluhe Basin, Qinghai-Tibet Plateau. Geomorphology 340, 1–14. doi: 10.1016/j.geomorph.2019.04.032.

Liu, F., Chen, L., Abbott, B.W., Xu, Y., Yang, G., Kou, D., Qin, S., Strauss, J., Wang, Y., Zhang, B., Yang, Y., 2018. Reduced quantity and quality of SOM along a thaw sequence on the

Tibetan Plateau. Environmental Research Letters 13, 104017. doi: 10.1088/1748-9326/aae43b.

Liu, F., Kou, D., Chen, Y., Xue, K., Ernakovic, J.G., Chen, L., Yang, G., Yang, Y., 2021. Altered microbial structure and function after thermokarst formation. Global Change Biology, 27, 4, 823-835. doi: 10.1011/gcb.15438.

Liu, F., Qin, S., Fang, K., Chen, L., Peng, Y., Smith, P., Yang, Y., 2022. Divergent changes in particulate and mineral-associated organic carbon upon permafrost thaw. Nature Communications, 13: 5073. doi: 10.1038/s41467-022-32681-7.

Lugato, E., Morari, F., Nardi, S., 2009. Relationship between aggregate pore size distribution and organic-humic carbon in contrasting soils. Soil and Tillage Research, 103, 153–157. doi: 10.1016/j.still.2008.10.013.

Lugato, E., Simonetti, G., Morari, F., Nardi, S., Berti, A., Giardini, L., 2010. Distribution of organic and humic carbon in wet-sieved aggregates of different soils under long-term fertilization experiment. Geoderma, 157: 80-85. doi: 10.1016/j.geoderma.2010.03.017.

Mako, A., Szabo, B., Rajkai, K., Szabo, J., Bakacsi, Z., Labancz, V., Hernadi, H., Barna, G., 2019. Evaluation of soil texture determination using soil fraction data resulting from laser diffraction method. International Agrophysics, 33, 4, 445-454. doi: 10.31545/intagr/113347.

Ma, R., Jiang, Y., Liu, B., Fan, H., 2021. Effects of pore structure characterized by synchrotron-based micro-computed tomography on aggregate stability of black soil under freeze–thaw cycles. Soil and Tillage Research 207, 104855. doi: 10.1016/j.still.2020.104855.

Ma, Y., Xie, T., Li, X., 2022. Spatial variation of soil organic carbon in the Qinghai Lake watershed, northeast Qinghai-Tibet Plateau. Catena, 213, 106187. doi: 10.1016/j.catena.2022.106187.

Mu, C., Abbott, B.W., Norris, A.J., Mu, M., Fan, C., Chen, X., Jia, L., Yang, R., Zhang, T., Wang, K., Peng, X., Wu, Q., Guggenberger, G., Wu, X., 2020. The status and stability of permafrost carbon on the Tibetan Plateau. Earth-Science Reviews, 211, 103433. doi: 10.1016/j.earthscirev.2020.103433.

Ozlu, E., Arriaga, F.J., 2021. The Role of Carbon Stabilization and Minerals on Soil Aggregation in Different Ecosystems. Catena 202, 105303. Doi: 10.1016/j.catena.2021.105303.

Oztas, T., Fayetorbay, F., 2003. Effect of freezing and thawing processes on soil aggregate stability. Catena 52 (1), 1–8. doi: 10.1016/S0341-8162(02)00177-7.

Patel, K.F., Tatariw, C., Macrae, J.D., Ohno, T., Nelson, S.J., Fernandez, I.J., 2021. Repeated freeze–thaw cycles increase extractable, but not total, carbon and nitrogen in a Maine coniferous soil. Geoderma, 402, 115353. doi: 10.1016/j.geoderma.2021.115353.

Peng, X.Q., Zhang, T.J., Frauenfeld, O.W., Wang, K., Cao, B., Zhong, X., Su, H., Mu, C., 2017. Response of seasonal soil freeze depth to climate change across China. Cryosphere, 11(3): 1059-1073. doi: 10.5194/tc-11-1059-2017.

Qiao, L., Zhou, H., Wang, Z., Li, Y., Chen, W., Wu, Y., Liu, G., Xue, S., 2023. Variations in soil aggregate stability and organic carbon stability of alpine meadow and shrubland under long-term warming. Catena 222, 106848. Doi: 10.1016/j.catena. 2022.106848.

Quigley, M.Y., Negassa, W.C., Guber, A.K., Rivers, M.L., Kravchenko, A.N., 2018. Influence of pore characteristics on the fate and distribution of newly added carbon. Frontiers in Environmental Science, 6:51. doi: 10.3389/fenvs.2018.00051.

Rabot, E., Wiesmeier, M., Schlute, S., Vogel, H.J., 2018. Soil structure as an indicator of soil functions: A review. Geoderma 314, 122-137. doi: 10.1016/j.geoderma.2017.11.009.

Rempel, A.W., van Alst, L.J., 2013. Potential gradients produced by pore-space heterogeneities: Application to isothermal frost damage and submarine hydrate anomalies. Poromechanics V: Proceedings of the Fifth Biot Conferences on Poromechanics, 813–822. doi: 10.1061/9780784412992.098.

Ruamps, L.S., Nunan, N., Pouteau, V., Leloup, J., Raynaud, X., Roy, V., Chenu, C., 2013. Regulation of soil organic C mineralisation at the pore scale. FEMS Microbiology Ecology, 86 (1), 26–35. doi: 10.1111/1574-6941.12078.

Schluter, S., Leuther, F., Albrecht, L., Hoeschen, C., Kilian, R., Surey, R., Mikutta, R., Kaiser, K., Mueller, C.W., Vogel, H., 2022. Microscale carbon distribution around pores and particulate organic matter varies with soil moisture regime. Nature Communications 13: 2098. Doi: 10.1038/s41467-022-29605-w.

Schutter, M.E., Dick, R.P., 2002. Microbial community profiles and activities among aggregates of winter fallow and cover-cropped soil. Soil Science Society of America Journal, 66 (1), 142-153. doi: 10.2136/sssaj2002.1420.

Schuur, E.A.G., Mack, M.C., 2018. Ecological response to permafrost thaw and consequences for local and global ecosystem services Annual Reviews of Ecology, Evolution, and Systematics 2018, 49, 279-301. doi: 10.1146/annurev-ecolsys-121415-032349.

Six, J., Bossuyt, H., Degryze, S., Denef, K., 2004. A history of research on the link between (micro)aggregates, soil biota, and soil organic matter dynamics. Soil and Tillage Research, 79(1):7-31. doi: 10.1016/j.still.2004.03.008

Six, E., Elliott, E., Paustian, K., 2000. Soil macroaggregate turnover and microaggregate formation: a mechanism for C sequestration under no-tillage agriculture. Soil Biology and Biochemistry, 32(14):2099-2103. doi: 10.1016/S0038-0717(00)00179-6.

Skvortsova, E.B., Shen, E.V., Abrosimov, K.N., 2018. The impact of multiple freeze–thaw cycles on the microstructure of aggregates from a Soddy-Podzolic soil: a microtomographic analysis. Eurasian Soil Science, 51 (2), 190-198. doi: 10.1134/S106422931802012.

Song, Y., Zou, Y., Wang, G., Yu, X., 2017. Altered soil carbon and nitrogen cycles due to the freeze-thaw effect: A meta-analysis. Soil Biology and Biochemistry, 109: 35-49. doi: 10.1016/j.soilbio.2017.01.020.

Starkloff , T., Larsbo, M., Stolte, J., Hessel, R., Ritsema, C., 2017. Quantifying the impact of a succession of freezing-thawing cycles on the pore network of a silty clay loam and a loamy sand topsoil using X-ray tomography. Catena, 156, 365–374. doi:10.1016/ j.catena.2017.04.026

Strong, E.T., Wever, H.D., Merckx, R., Recous, S., 2004. Spatial location of carbon decomposition in the soil pore system. European Journal of Soil Science, 55 (4), 739–750. doi: 10.1111/j.1365-2389.2004.00639.x.

Sun, T., Mao, X., Han, K., Wang, X., Cheng, Q., Liu, X., Zhou, J., Ma, Q., Ni, Z., Wu, L., 2023. Nitrogen addition increased soil particulate organic carbon via plant carbon input whereas reduced mineral-associated organic carbon through attenuating mineral protection in agroecosystem. Science of the Total Environment, 165705. doi: 10.1016/j.scitotenv.2023.165705.

Tan, B., Wu, F., Yang, W., He, X., 2014. Snow removal alters soil microbial biomass and enzyme activity in a Tibetan alpine forest. Applied Soil Ecology, 76, 34–41. doi: 10.1016/j.apsoil.2013.11.015.

Tarnocai, C., Canadell, J.G., Schuur, E.A.G., Kuhry, P., Mazhitova, G., Zimov, S., 2009. Soil organic carbon pools in the northern circumpolar permafrost region. Global Biogeochemical Cycles 23(2), GB2023. doi: 10.1029/2008GB003327.

Todd-Brown, K.E.O., Randerson, J.T., Hopkins, F., Arora, V., Hajima, T., Jones, C., Shevliakova, E., Tjiputra, J., Volodin, E., Wu, T., Zhang, Q., Allison, S.D., 2014. Changes in soil organic carbon storage predicted by Earth System models during the 21st century. Biogeosciences, 11 (8): 2341-23356. doi: 10.5194/bg-11-2341-2014.

Toosi, E.R., Kravchenko, A.N., Guber, A.K., Rivers, M.L., 2017. Pore characteristics regulate priming and fate of carbon from plant residue. Soil Biology and Biochemistry, 113, 219–230. doi: 10.1016/j.soilbio.2017.06.014.

Védère, C., Vieublé Gonod, L., Pouteau, V., Girardin, C. & Chenu, C., 2020. Spatial and temporal evolution of detritusphere hotspots at different soil moistures. Soil Biology and Biochemistry 150, 107975. doi: 10.1016/j.soilbio.2020.107975.

Wang, D., Ma, Y., Niu, Y., Chang, X., Wen, Z., 2007. Effects of cyclic freezing and thawing on mechanical properties of Qinghai-Tibet clay. Cold Regions Science and Technology, 48:34–43. doi: 10.1016/j.coldregions. 2006. 09. 008

Wang, E., Cruse, R., Chen, X., Daigh, A., 2012. Effects of moisture condition and freeze/thaw cycles on surface soil aggregate size distribution and stability. Canadian Journal of Soil Science, 92 (3), 529-536. doi: 10.1007/s40333-017-0009-3.

Wang, M., Guo, X., Zhang, S., Xiao, L., Mishra, U., Yang, Y., Zhu, B., Wang, G., Mao, X., Qian, T., Jiang, T., Shi, Z., Luo, Z., 2022. Global soil profiles indicate depth-dependent soil carbon losses under a warmer climate. Nature Communications 13, 5514. doi: 10.1038/s41467-022-33278-w.

Wang, R., Hu, X., 2024. Pore structure characteristics and organic carbon distribution of soil aggregates in alpine ecosystems in the Qinghai Lake basin on the Qinghai-Tibet Plateau. Catena 231, 107359. doi: 10.1016/j.catena.2023.107359.

Wang, X., Wang., C., Fan, X., 2024. Mineral composition controls the stabilization of microbially derived carbon and nitrogen in soils: Insights from an isotope tracing model. Global Change Biology 30 (1): e17156. doi: 10.1111/gcb.17156.

Wang, Y., Li, S., Xu, Y., 2020. Incorporated maize residues will induce more accumulation of new POC in HF compared with that in LF soils: a comparison of different residue types. Journal of Soil and Sediments, 20, 3941–3950. doi: 10.1007/s11368-020-02718-9.

Witzgall, K., Vidal, A., Schubert, D.I., Hoschen, C., Schweizer, S.A., Buegger, F., Pouteau, V., Chenu, C., Mueller, C.W., 2021. Particulate organic matter as a functional soil component for persistent soil organic carbon. Nature Communications, 12 (1), 1–10. doi: 10.1038/s41467-021-24192-8.

Wu, Q., Zhang, T., Liu, Y., 2010. Permafrost temperatures and thickness on the Qinghai-Tibet Plateau. Global and Planetary Change, 72 (1–2), 32–38. doi: 10.1016/j.gloplacha.2010.03.001.

Wu, T., Li., X., Zuo, F., Deng, Y., Hu, G., 2023. Responses of soil water dynamics to precipitation events in an alpine meadow ecosystem of the Qinghai Lake Basin based on high-precision lysimeter measurements. Hydrological Processes, 37(4): e14874. doi: 10.1002/hyp.14874.

Wu, Y., Hu, X., 2024. Soil open pore structure regulates soil organic carbon fractions of soil aggregates under simulated freeze-thaw cycles as determined by X-ray computed tomography. Journal of Soil Science and Plant Nutrition. doi: 10.1007/s42729-024-01904-9.

Xiao, L., Zhang, Y., Li, P., Xu, G., Shi, P., Zhang, Y., 2019. Effects of freeze–thaw cycles on aggregate-associated organic carbon and glomalin-related soil protein in natural-succession grassland and Chinese pine forest on the Loess Plateau. Geoderma, 334, 1–8. doi: 10.1016/j.geoderma.2018.07.043.

Yang, Z., Hu, X., Gao, Z., Zhao, Y., 2021. Soil macropore networks derived from X-ray computed tomography in response to typical thaw slumps in Qinghai-Tibetan Plateau, China. Journal of Soil and Sediments, 21, 2845-2854. doi: 10.1007/s11368-021-02983-2

Yi, Y., Kimball, J.S., Rawlins, M.A., Moghaddam, M., Euskirchen, E.S., 2015. The role of snow cover affecting boreal-arctic soil freeze–thaw and carbon dynamics. Biogeosciences, 12:5811–5829. doi: 10.5194/bg-12-5811-2015.

Zhang, W., Munkholm, L.J., Liu, X., An, T., Xu, Y., Ge, Z., Xie, N., Li, A., Dong, Y., Peng, C., Li, S., Wang, J., 2023. Soil aggregate microstructure and microbial community structure mediate soil organic carbon accumulation: Evidence from one-year field experiment. Geoderma, 430, 116324. doi: 10.1016/j.geoderma.2023.116324.

Zhao, Y., Hu, X., 2022. How do freeze–thaw cycles affect the soil pore structure in alpine meadows considering soil aggregate and soil column scales? Journal of Soil Science and Plant Nutrition 22, 4207-4216. doi: 10.1007/s42729-022-01019-z.

Zhang, X., Xin, X., Zhu, A., Zhang, J., Yang, W., 2017. Effects of tillage and residue managements on organic C accumulation and soil aggregation in a sandy loam soil of the North China Plain. Catena, 156, 176–183. doi: 10.1016/j.catena.2017.04.012.

Zhang, Z., Wei, M., Feng, W., Xiao, D., Hou, X., 2016. Reconstruction of soil particle composition during freeze-thaw cycling: A review. Pedosphere 26 (2), 167-179. doi: 10.1016/S1002-0160(15)60033-9.

Zhao, Y., Hu, X., 2023a. A pore-scale investigation of soil aggregate structure responding to freeze–thaw cycles using X-ray computed microtomography. Journal of Soils and Sediments 23, 3137-3148. doi: 10.1007/s-11368-022-03539-2.

Zhao, Y., Hu, X., 2023b. Seasonal freeze–thaw processes regulate and buffer the distribution of microbial communities in soil horizons. Catena, 231, 107348. doi: 10.1016/j.catena.2023.107348.

Zhao, Y., Hu, X., Li, X., 2020. Analysis of the intra-aggregate pore structures in three soil types using X-ray computed tomography. Catena, 193, 104622. doi: 10.1016/j.catena.2020.104622.

Zhou, H., Peng, X., Peth, S., Xiao, T., 2012. Effects of vegetation restoration on soil aggregate microstructure quantified with synchrotron-based micro-computed tomography. Soil and Tillage Research 124: 17-23. doi: 10.1016/j.still.2012.04.006.

Zhu, E., Li, Z., Ma, L., 2024. Enhanced mineral preservation rather than microbial residue production dictates the accrual of mineral-associated organic carbon along a weathering gradient. Geophysical Research Letters 51(6): e2024GL108466. doi: 10.1029/2024GL108466.

Figure Captions

Fig. 1. Location of the sampling site (a) and landscapes of the *Kobresia pygmaea* meadow ecosystem (b) and the *Potentilla fruticosa* shrub ecosystem (c).

Fig. 2. Daily average soil temperature in 2021 and the classification of freeze–thaw stages (SFP-stable frozen period, UTP-unstable thawing period, STP-stable thawing period and UFP-unstable freezing period).

Fig. 3. Procedures used for the visualization and quantification of soil aggregate pore networks. Taken from Zhao et al. (2020) with permission from Elsevier.

Fig. 4. Pore size distribution (by pore diameter) of soil aggregates in the (a) meadow ecosystem and (b) shrubland ecosystem during the seasonal FT process. Bars represent the mean ± standard error (n=18). Different lowercase letters denote significant differences among pore volume percentages in different FT periods ($P<0.05$).

Fig. 5. Pore characteristics of soil aggregates during the seasonal FT process. (a) porosity, (b) pore equivalent diameter, (c) mean volume of pores, (d) pore surface area density, (e) pore length density and (f) pore shape factor. Bars represent the mean ± standard error (n=9). ** represents significant differences between pore characteristics in freezing period and thawing period ($P<0.05$). Different lowercase letters denote significant differences between pore characteristics of >2 mm aggregates and 0.25-2 mm aggregates ($P<0.05$).

Fig. 6. Changes of SOC content (a-TOC, b-POC and c-MAOC) of soil aggregates during the seasonal freeze–thaw process. Bars represent the mean ± standard error (n=9). Different lowercase letters denote significant differences among SOC contents in different FT periods ($P<0.05$).

Fig. 7. Scatter plots of relationships between (a) SOC content and 15-30 μm pores and (b) SOC content and > 80 μm pores in the freezing process.

Fig. 8. Scatter plots of relationships between (a) TOC content and pore length density, (b) MAOC content and pore length density and (c) POC content and < 15 μm pores in the thawing process.

Supplementary Data

Supplementary Table 1. Basic soil physio-chemical properties

Ecosystem	Soil depth (cm)	Bulk density (g/cm³)	Soil water content (%)	pH	Organic C (g/kg)	Total N (g/kg)	Particle size composition (%)		
							clay	silt	sand
KPM (meadow)	0-10	0.77±0.19b	35.76±15.01	6.50±0.35	85.26±29.38a	7.66±2.22a	9.05±2.65	33.60±6.10	57.35±8.73
	10-30	1.00±0.17a	32.00±20.68	6.49±0.19	67.12±20.49ab	6.94±1.37ab	10.65±3.74	35.83±9.05	53.52±12.64
	30-50	1.07±0.05a	24.18±13.04	7.17±0.32	25.35±6.78b	2.66±0.45b	11.84±2.57	34.88±4.98	53.28±7.32
PFS (shrubland)	0-10	0.83±0.23	42.57±4.57a	6.64±0.40	64.42±11.22a	7.00±1.12a	13.95± 0.56	47.56± 1.25	38.49± 1.69
	10-30	0.81±0.15	32.40±8.70ab	6.82±0.22	44.11±6.88ab	4.30±0.90ab	14.59± 0.86	46.85± 1.00	38.56± 1.73
	30-50	0.96±0.15	22.82±0.50a	7.31±0.37	36.44±7.06b	3.38±0.53b	15.05± 1.80	47.44± 3.80	37.50± 5.58

Note: KPM-*Kobresia pygmaea* meadow; PFS- *Potentilla fruticosa* shrub. The properties were measured with samples taken in the unstable freezing period. All data is presented with standard error (n=3). Different lowercase letters denote significant difference between soil layers.

Supplementary Table 2. Mass proportions of soil aggregates in alpine ecosystems during the seasonal freeze–thaw process

Ecosystem	Aggregate fraction	Mass proportion of aggregates (%)			
		UFP	SFP	UTP	STP
KPM (meadow)	> 2 mm	34.55±6.80ab	41.14±11.36a	29.83±8.72b	38.86±12.90ab
	0.25-2 mm	46.29±5.60a	37.29±7.77b	48.73±6.86a	42.97±11.81ab
	0.053-0.25 mm	16.61±3.64	16.73±5.73	20.27±4.32	15.56±5.09
	<0.053 mm	2.55±0.80a	4.84±2.74a	1.16±0.81b	2.61±1.61ab
PFS (shrubland)	> 2 mm	32.17±5.49	34.52±13.59	26.57±6.66	30.03±8.52
	0.25-2 mm	47.30±5.80a	35.40±6.50b	51.72±8.65a	45.02±7.17a
	0.053-0.25 mm	18.07±3.28b	22.50±7.40a	18.72±4.28ab	21.00±7.10ab
	<0.053 mm	2.49±1.62ab	7.75±3.50a	2.92±2.16b	3.95±3.52ab

Note: Bars represent the mean ± standard error (n=9). Uppercase letters represent significant differences among FT periods ($P<0.05$).

Supplementary Table 3 Correlations between SOC content and soil structure of soil aggregates in freezing period and thawing period

	Thawing period									
	Porosity	Equivalent diameter	Mean volume	Pore surface area density	Pore length density	Pore shape factor	Pd<15	Pd15-30	Pd30-80	Pd>80
TOC	0.428	-0.404	-0.124	0.553	**0.718***	0.241	0.420	0.084	0.316	-0.235
POC	0.222	-0.252	0.188	0.339	0.397	0.032	**0.639***	0.123	0.410	-0.273
MAOC	0.529	-0.443	-0.479	**0.622***	**0.865****	0.422	0.013	0.010	0.086	-0.106
	Freezing period									
	Porosity	Equivalent diameter	Mean volume	Pore surface area density	Pore length density	Pore shape factor	Pd<15	Pd15-30	Pd30-80	Pd>80
TOC	0.582	-0.507	-0.036	0.326	0.396	0.199	**0.811***	**-0.834****	-0.503	**0.733***
POC	0.521	-0.214	-0.274	0.178	0.428	0.538	0.458	-0.353	-0.146	0.295
MAOC	0.409	-0.498	0.117	0.296	0.234	0.071	**0.727***	**-0.818***	-0.532	**0.727***

Note: * represents the correlation is significant (P<0.05). Pd<15: volume percentage of pores <15 μm, Pd15-30: volume percentage of pores 15-30 μm; Pd30-80: volume percentage of pores 30-80 μm; Pd>80: volume percentage of pores >80 μm.

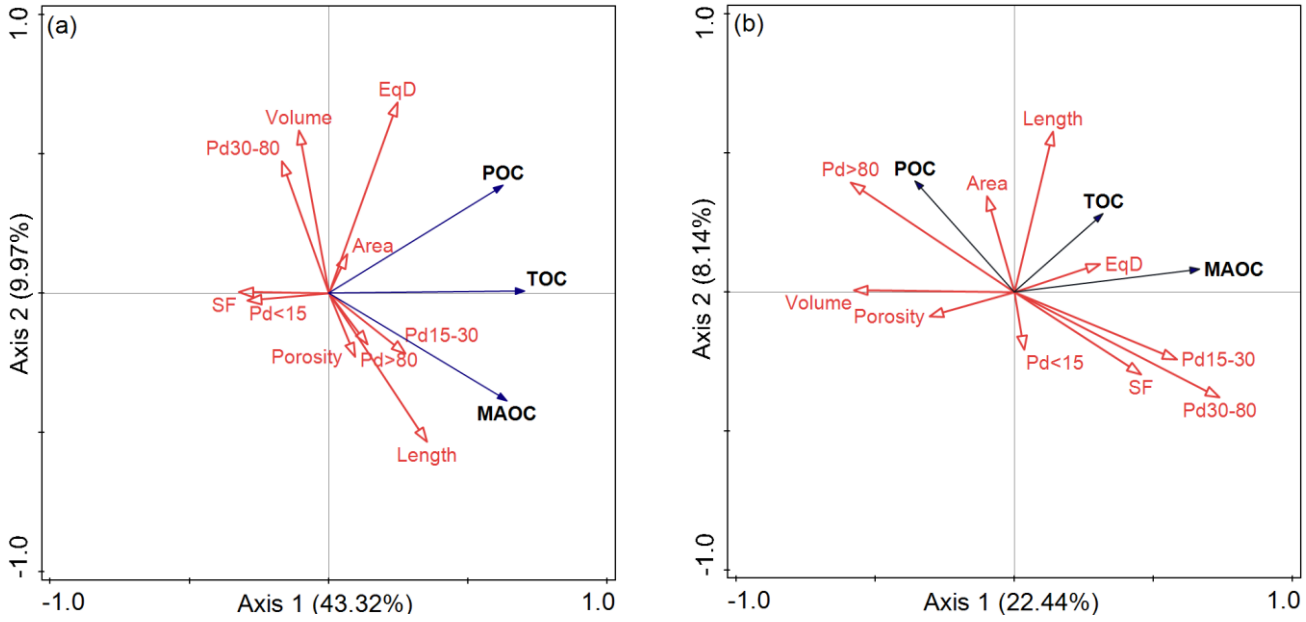

Supplementary Figure 1. RDA analysis between SOC content and pore characteristics of aggregates in (a) the freezing period and (b) the thawing period.

Note: Volume-pore volume, EqD-equivalent diameter of pores, Pd30-80-pores with diameter of 30-80 μm, SF-pore shape factor, Pd<15: pores with diameter of <15 μm, Pd15-30- pores with diameter of 15-30 μm, Pd>80- pores with diameter of > 80 μm.